Thin film composite hollow fibre membrane

for pharmaceutical concentration and solvent recovery

Keng Siang Goh[a], Yunfeng Chen[a], Jeng Yi Chong[a], Tae Hyun Bae[b], Rong Wang [a, c, *]

[a] Singapore Membrane Technology Centre, Nanyang Environment and Water Research Institute, Nanyang Technological University, 1 Cleantech Loop, Singapore 637141, Singapore

[b] Department of Chemical and Biomolecular Engineering, Korea Advanced Institute of Science and Technology, Daejeon 34141, Republic of Korea

[c] Singapore of Civil and Environmental Engineering, Nanyang Technological University, 50 Nanyang Avenue, Singapore 639798, Singapore

* Corresponding author. Email address: rwang@ntu.edu.sg

Highlights

- 100-piece thin-film composite OSN membrane was successfully fabricated
- 7-day filtration test showed stable organic solvent nanofiltration (OSN) performance
- High acetone permeability of 24.2 l m^{-2} h^{-1} bar^{-1} and 90.1% methyl red rejection
- Active pharmaceutical ingredient was concentrated to 2 wt%

Abstract

A 100-piece hollow fibre thin-film composite membrane module was successfully developed for pharmaceutical concentration and solvent recovery. To increase its packing density, thinner P84 polyimide hollow fibre substrates were spun using a smaller spinneret. The substrates were subsequently cross-linked with hexamethylene diamine to achieve organic solvent resistance. An MPD-based thin-film composite was synthesized through interfacial polymerisation to increase selectivity for solutes of less than 300 Da. The thin-film composite was then solvent-activated using N,N-dimethylformamide to increase its solvent permeability. The resulting membrane exhibited excellent performance with 24.2 l m^{-2} h^{-1} bar^{-1} acetone permeability and 90.1% methyl red (269 Da) rejection. In addition, the solvent-activated membrane maintained its performance for prolonged period, demonstrating the scalability of the thin-film composite fabrication process and stability of solvent-activated membranes. The membrane was also able to concentrate levofloxacin (361 Da) from 500 ppm to 20,000 ppm in acetone using a batch process, showing promising results for pharmaceutical applications.

1. Introduction

Membrane technology has revolutionized water treatment for municipal and industrial applications in the past few decades. Similarly, organic solvent nanofiltration (OSN) is being touted as a potential replacement or augmentation to conventional processes handling organic solvents in various industries due to its unique advantages [1-3]. For instance, OSN addresses the limitations of distillation and evaporative processes used in purification and recovery systems, where high energy consumption and intense processing conditions are required [4]. OSN, a pressure-driven membrane process, enables thermally sensitive products in the feed stream to be purified to high level without the risk of thermal degradation [3, 5-9]. In addition, the energy consumption is also significantly lesser as there is no change in phase of the feed stream. The milder operating conditions of the system also mean that the cost of constructing the system can be kept low. Furthermore, OSN membrane systems can be installed modularly into existing separation processes to form a hybrid system, thereby encouraging the uptake of such technology in existing plants [7, 9]. Just like how reverse osmosis (RO) membranes replaced thermal desalination for water purification, OSN membranes will continue to be refined with the goal of one day replacing existing industrial processes for solvent purification and recovery.

New types of polymers were developed for OSN applications over the past few decades. Polymeric membranes made of polybenzimidazole (PBI), polyether ether ketones (PEEK), polymer with intrinsic microporosity (PIM) and polyimides exhibit excellent chemical and thermal stability, vastly expanding their industrial applications [1, 3, 7, 9-11]. New fabrication and treatment techniques have also enhanced the tuneable properties of the membranes, increasing both permeability and selectivity. One such technique is the cross-linking of polymeric membranes, which was frequently discussed in literature and eventually used in commercialised membranes [8, 12, 13]. This process enhances the chemical and thermal stability of polymeric

membranes and made them suitable to use in feed streams with harsh conditions. Another method was also developed to prepare highly permeable OSN membranes in one-step process. Cross-linked polymeric membranes with low permeability underwent solvent annealing, resulting in several times higher solvent permeances with little compromise on selectivity [8, 13, 14]. This method has been applied for improving the performance of commercial membranes such as Duramem 300 from Evonik [13]. In addition, studies on membrane surface modifications were reported to improve the selectivity and permeability of OSN membranes. Membrane surfaces were functionalised or altered through methods such as grafting, radiation, plasma-induced treatment, polyelectrolyte layering and interfacial polymerisation [15, 16]. One of the more established modification techniques, interfacial polymerisation (IP), has been implemented in RO membranes for water desalination and proves to be a viable modification technique for OSN membranes [14, 17-20].

Since the early 2000s, several OSN applications have been studied and subsequently implemented in small scale, such as solvent exchange in multi-step chemical processes, purification of active pharmaceutical ingredients (APIs) and solvent recovery from manufacturing processes [21-25]. The first ever large-scale implementation of OSN technology was in solvent lube dewaxing [26]. The membrane-based process led to significant decrease in water and energy consumptions, as well as achieving a higher yield of lube oil. Another potential use of OSN technology is in the pharmaceutical industry due to its solvent intensive processes [1, 7, 25, 27]. The separation of high-value APIs from impurities using conventional distillation techniques requires large amounts of energy and solvents, resulting in a high operating cost to obtain the end products [1]. Thus, the pharmaceutical industry can benefit tremendously from the implementation of OSN technology in several stages in the API manufacturing process. For example, membrane technology can be used to recover the catalyst in batch reaction processes. This can open more possibilities of using

thermal sensitive catalysts that cannot be recovered through evaporative techniques. Another potential use of OSN in API production is the purification of intermediaries prior to solvent exchange. Additionally, a large amount of key output materials (KOM) may be lost during the crystallisation and purification step. A highly selective OSN membrane can potentially result in a higher yield of the KOM and thereby reducing wastage [27]. OSN membranes can also be used is the recovery of solvents used in the process chain. In a life cycle analysis on API production, it was reported that organic solvents represent the largest amount of raw materials required for API production at more than 95% by mass [27]. Thus, there is a need to recover these organic solvents to reduce waste production, potentially lowering the economic and environmental costs of the manufacturing process. However, several issues need to be addressed before OSN technology can revolutionize the pharmaceutical industries, just like RO membranes in water treatment processes.

Firstly, current state-of-the-art technologies for OSN membranes are not easily scalable, preventing it from being commercialised [4]. There is a need to develop a streamlined OSN membrane manufacturing process that emphasizes on engineering feasibility and economic viability. Secondly, novel materials such as nanocomposites and filler materials used in OSN membrane fabrication have not been demonstrated to offer performance stability over prolonged operations [28]. The leaching of such nanoparticles may contaminate the permeate, rendering the recovered solvent unsuitable for reuse. Lastly, more emphasis should be focused on improving the selectivity of the membranes. Commercial OSN membranes need to exhibit better separation characteristics for solutes around 300 Da, the typical range of molecular weights for APIs [1]. In addition, typical pharmaceutical feed streams consist of multiple solutes. An incomplete separation of these solutes from the APIs renders OSN membranes less viable in replacing currently proven purification technologies. The partial rejection of solutes in the solvent recovery steps also meant that the permeate obtained cannot be reused in industrial processes where

contaminant-free solvents are required [1]. With these issues in mind, lessons can be learnt from how membranes developed for water applications have been refined over the years.

Most commercial OSN membranes are integrally skinned asymmetric (ISA) membranes rather than thin-film composites (TFC). Though ISA membranes are easier to fabricate compared to TFC membranes, the latter boasts superior solvent permeability and selectivity. A typical selective layer of the TFC membranes used for brackish water and seawater treatments is m-phenylenediamine (MPD)-based polyamide. It is synthesized using interfacial polymerization (IP), where a polymeric selective layer is formed through the reaction of two or more monomers at an immiscible liquid interface. It has been widely used in RO and this well-established technology can be implemented in OSN to ensure scalability and reliability of developed membranes [29, 30]. Another well-established technology that OSN can benefit from is the use of hollow fibre membranes. Compared to flat sheet membranes, hollow fibre membranes demonstrate higher packing density and surface area to volume ratio as well as self-supporting capability [31], which reduce the infrastructure footprint required to implement the modular system for existing plants. Since most commercial OSN membranes are in flat sheet configuration, developing hollow fibre OSN membranes can provide more options for industries. In our previous study, a polyamide-based TFC hollow fibre membrane was successfully fabricated and proved to be viable for use in certain OSN application [17], but the module size was small. There is a need to further develop this technology to enhance its performance and scalability, paving the way for practical applications of OSN membranes.

In this work, a more selective TFC hollow fibre membrane module was developed for target applications in the pharmaceutical industry. P84 polyimide substrate was used as the substrate as it has been proven to be solvent resistant in several commonly used organic solvents such as

isopropanol and acetone [17]. In addition, the chemical cross-linking process used was easily scalable and facile [32]. The substrate fabricated in previous work was further improved to increase the performance of the overall TFC membrane by adjusting its spinning parameters. To increase the selectivity of the TFC membrane for smaller (< 300 Da) solutes, the monomers used in the IP step was changed from a combination of piperazine (PIP)/polyetherimide (PEI)/PEI to MPD, and the IP process was carefully adjusted to obtain a denser selective layer. This is expected to reduce the loss of valuable API during the concentration process and improve the purity of the recovered solvent. The permeability of the membrane was enhanced through solvent activation by DMF, opening up the pores of the selective layer and substrate while maintaining excellent rejection of solutes. To determine the scalability of the TFC fabrication process, the performance of a 5-piece module was compared with a 100-piece module. In addition, 7-day stability of the 100-piece module was also carried out to study the stability of the solvent-activated TFC membrane under operating conditions. Lastly, an API with a relatively small molecular weight was concentrated in a batch process and the organic solvent was recovered simultaneously. Overall, this study explored the scalability and stability of the TFC OSN membrane and its potential use in pharmaceutical industry.

2. Materials and methods

2.1 Materials

Polyimide (P84 Lenzing) was used to fabricate the substrate. 1-Methyl-2-pyrrolidinone (NMP, >99%, Merck) and diethylene glycol (DG, >99.5%, Sigma Aldrich) were used in the phase inversion process. Isopropanol (IPA, >99.5%, Sigma Aldrich), polyethylene glycol 400 (PEG 400, Sigma Aldrich) and hexamethylene diamine (HDA, >98%, Sigma Aldrich) were used for post-treatment and storage of membranes. For the IP process, m-phenylenediamine (MPD, >99%,

Sigma Aldrich), cyclohexane (>99%, VWR) and Benzene tricarbonyl trichloride (TMC, >98%, Sigma Aldrich) were used.

To evaluate the rejection capability of the TFC membranes, rose bengal (1017 Da in molecular weight (MW), >95%, Sigma Aldrich), acid fuchsin (585 Da in MW, ~70%, Sigma Aldrich) and methyl orange (327 Da in MW, > 85%, Sigma Aldrich), methyl red (269 Da in MW, ACS reagent) and levofloxacin (361 Da in MV, >98%, Sigma Aldrich) purchased from Sigma Aldrich were used. Acetone (>95%, Sigma Aldrich), acetonitrile (>99.5%, Sigma Aldrich), isopropanol (IPA, >99.5%, Sigma Aldrich) and N,N-dimethylformamide (DMF, >99.8%, Sigma Aldrich) were used in the solute-solvent system.

2.2 Fabrication of hollow fibre membrane module

P84 polyimide hollow fibre substrate was spun in-house using the method described previously [16] and cross-linked with HDA to achieve organic solvent resistance. P84 polymer was first dried in a 60°C oven for 24 hours prior to dope preparation. The dope was prepared by mixing P84 polyimide with DG and NMP in a 20/8/72 weight percent, respectively. The dope solution was stirred continuously in a water bath at 50°C for 24 hours before being transferred to a syringe pump and degassed overnight. The P84 polyimide hollow fibre substrate was spun using the dry-jet wet spinning process according to the following conditions (Table 1). The spinning parameters from the previous work were further improved in this study to increase the performance of the substrate. For example, a smaller spinneret was used to increase its packing density for future scale-up works. In addition, a harder bore fluid and lower air gap were used to increase the extent of finger-like structures from the inner and outer surfaces of the membrane.

Table 1: Spinning condition for P84 hollow fibre

Parameters	This work	Previous work [17]
Spinneret (mm/mm)	0.5/1.0	0.75/1.5
Dope flow rate (ml/min)	3	3.5
Bore fluid	de-ionised water (DI)	NMP/DI (30/70) wt%
Bore fluid flow rate (ml/min)	3	3
External coagulant	Tap water	Tap water
Coagulant temperature (˚C)	24	24
Air gap (cm)	5	20

A spinneret with inner and outer diameters of 0.5 mm and 1.0 mm, respectively, was used to produce finer fibres for higher packing density. The as-spun polyimide substrates were cross-linked by submerging it into a solution of 20 g/l of HDA in IPA for 18 hours. The solution is circulated constantly to ensure complete cross-linking [17].

The organic solvent resistant substrates were then potted into two different sets of modules and sealed at both ends with organic solvent resistant epoxy. The two sets of modules have an effective length of 0.22 m and 0.36 m, respectively. In addition, the first set of modules contain 5 fibres each while the longer module contains 100 fibres each.

After the hollow fibre substrates were potted into modules, interfacial polymerisation was carried out to produce a polyamide selective layer. The selective layer was synthesized on the inner surface of the hollow fibres through in-house interfacial polymerisation process described in our

previous work [17]. However, PEI/PIP aqueous monomers were replaced with MPD to achieve a tighter selective layer. The modules were first soaked in MPD solution and then purged with cyclohexane to remove excess MPD. A TMC solution was then pumped through the lumen to form a thin polyamide layer on the substrate. As the 100-piece module is longer and contains more fibres, a slightly higher crossflow rate of the solutions was used to reduce the dilution effect of reactants at the outlet. The modules were kept in DI for storage before use.

2.3 Membrane characterisation

The cross-section, inner and outer surfaces of the polyimide substrate and TFC membrane were examined under a Zeiss EVO 50 Scanning Electron Microscope (SEM). Hollow fibre samples were first dried, then fractured in liquid nitrogen and coated with platinum using EMITECH SC7620 sputter coater for the SEM preparation.

To evaluate the cross-linking of the polyimide substrate, Fourier Transform Infrared Spectroscopy (FTIR) was carried out using Prestige-21 spectrophotometer from Shimadzu. Typical polyimide bands at 1780 and 1711 cm^{-1} (C=O), 1361 cm^{-1} (C-N), and amide bands at 1634 cm^{-1} (C=O) and 1525 cm^{-1} (C-N) were identified to track changes to the polymer structure. To further confirm the presence of the polyamide TFC after the IP reaction, X-ray photoelectron spectroscopy (XPS) was performed using a Kratos AXIS Ultra.

Mechanical properties of the substrate were characterised by the tensile strength test using Zwick 0.5 kN Universal Testing Machine. Hollow fibre samples were clamped at both ends and pulled at 50 mm/min until breakage. The tensile modulus, yield stress and yield strain of the fibres were measured along with the elongation process.

The organic solvent resistant of the substrate was also determined by two tests. The weight loss of the membrane was examined before and after immersion in acetone, acetonitrile, IPA and DMF. The membranes were first dried in an oven at 60 °C for at least 24 hours and weighed. Then, the membranes were immersed in the respective solvents for 7 days, dried and weighed again. The weight loss was calculated using equation 1 with m_i and m_f (g) as the initial and final dry mass of the membrane, respectively.

$$Weight\ loss = \frac{m_i - m_f}{m_i} \times 100 \quad (1)$$

The degree of swelling of the membrane was also examined by measuring the change in length of the membrane when immersed in an organic solvent. The membranes were first cut into pieces each 0.1 m long and placed inside acetone, acetonitrile, IPA and DMF for 7 days before measuring the fibre length again. The degree of swelling can then be calculated using equation 2, where l_m and l_{m+s} are the length of dry membrane and solvent impregnated membrane, respectively.

$$Degree\ of\ swelling = \frac{l_m - l_{m+s}}{m_m} \times 100 \quad (2)$$

2.4 Membrane separation properties

A crossflow setup was used to carry out membrane performance tests to reduce concentration polarisation and excessive head-loss across membrane modules. The permeations of water, acetone, acetonitrile and IPA for the polyimide substrate and TFC membranes were evaluated by running the individual solvent from the lumen side at 2 bars. Measurements were taken only after 1 hour of conditioning was done for each solvent. The permeates were collected for at least 5 mins and the performances were calculated using equation 3, where J_i (l m^{-2} hr^{-1} bar^{-1}) is the permeability of water, acetone, acetonitrile or IPA, ΔP (bar) is the transmembrane pressure, A (m^2) is the effect area of the membrane, ρ_i (g cm^{-3}) is the density of water, acetone, acetonitrile or IPA, and t (h) is the time of permeate collected.

$$J_i = \frac{m_i}{\Delta P \times A \times \rho_i \times t} \quad (3)$$

The molecular weight cut-offs (MWCOs) of the polyimide substrate was evaluated by running a 2,000 ppm of dextran aqueous solution with molecular weight distribution ranging from 6k to 450k Da at 1 bar. Similarly, the permeates were collected after 1 hour of conditioning and measured using gel permeation chromatography (GPC) PL-GPC50 from Varian Inc. The rejections of each range of dextran molecules were calculated using equation 4, where R_i is the rejection coefficient for dextran molecule with certain molecular weight i, C_f and C_p (mV) are responses detected by the GPC for the feed and permeate solutions, respectively.

$$R_i = \frac{C_f - C_p}{C_f} \times 100 \quad (4)$$

The selectivity of the 5-piece or 100-piece module was measured by running acetone containing 50 ppm of rose bengal, acid fuchsin, methyl orange or methyl red, respectively, at 2 bar. The permeates were collected after 1 hour of conditioning and measured using a UV-1650 PC UV-Vis spectrophotometer from Shimadzu at 550 nm, 546 nm, 416 nm and 520 nm, respectively. The concentrations of dyes in acetone can then be calculated using Beer-Lambert's law. The calculated concentrations were then used to determine the membrane rejection for each dye using equation 4.

2.5 Effect of solvent activation on membrane separation properties

Solvent activation was performed on the 100-piece TFC module to examine its effect on selectivity and permeability. DMF was pumped at 1 bar from the lumen side for 5 min to activate the membranes. Subsequently, distilled water was pumped, without recirculation, at 1 bar from the lumen side for 10 min to flush out any remaining DMF in the membrane pores. The selectivity and permeability tests described in 2.4 were then carried out immediately after solvent activation.

2.6 7-day stability test and concentration of active pharmaceutical ingredients

A 7-day stability tests of the pristine and solvent-activated TFC membranes were conducted to study the performance of the 100-piece TFC module under prolonged organic solvent filtration. The selectivity and permeability were determined using 50 ppm of methyl red in acetone. Levofloxacin was concentrated using the pristine and solvent-activated TFC membranes to simulate their performance on pharmaceutical purification process. For the pristine TFC membrane, 50 ppm of levofloxacin was dissolved in acetone and concentrated to 20,000 ppm to replicate the API recovery process. Likewise, the solvent-activated TFC membrane was used to concentrate levofloxacin from 5,000 ppm to 20,000 ppm. The concentration of levofloxacin in the solutions was determined by HPLC analysis. It was carried out by Agilent HPLC system equipped with UV/vis detector set at a wavelength of 220 nm and a Discovery HS C18, 150 x 46 mm column. 25 mM potassium phosphate (pH 3.0) and acetonitrile were used as the mobile phase with 9:1 volumetric flow ratio. The solutions were pre-diluted to ensure that the concentration of levofloxacin is within the accurate range of the calibration curve.

3. Results and Discussion

3.1 Characterisation of P84 hollow fibre substrate

The MWCO of the cross-linked substrate was measured to be about 100 kDa, well within the range of pore size suitable for a defect-free polyamide synthesis onto the substrate [33]. The changes in physical properties of the membrane were observed as shown in Table 2. Compared to our previous work, the inner diameter of the membrane was reduced using a smaller spinneret [17], aiming at achieving a higher packing density, which is beneficial to future scaling-up of the membrane. The SEM images of the cross-linked substrate were also taken to examine its

morphology (Figure 1). As shown from Figure 1(A), the low air gap and hard bore fluid used in the spinning process resulted in the formation of finger-like macrovoids, extending from both the inner and outer surfaces of the hollow fibre membrane [34]. These finger-like structures are understood to weaken the mechanical strength of the membrane and render it unsuitable for use in various applications such as gas separation and reverse osmosis. However, it improves the low-pressure performance of the membrane by lowering its tortuosity and increasing its porosity [35]. In addition, the hard bore fluid also enabled the formation of a thin sponge-like layer on the inner surface which facilitates the formation of a defect-free selective layer through interfacial polymerisation (Figure 1(B & C)) [35, 36].

Table 2: Properties of membrane substrate before and after cross-linking

	Before cross-linking	**After cross-linking**
Inner diameter (μm)	677.2 ± 7.1	640.5 ± 5.2
Outer diameter (μm)	978.1 ± 9.6	920.4 ± 12.3
Thickness (μm)	150.5 ± 5.2	139.9 ± 7.7
Tensile modulus (MPa)	69.9 ± 5.0	79.7 ± 5.6
Stress (MPa)	6.30 ± 0.46	8.96 ± 0.70
Strain (%)	34.0 ± 1.4	22.4 ± 0.9

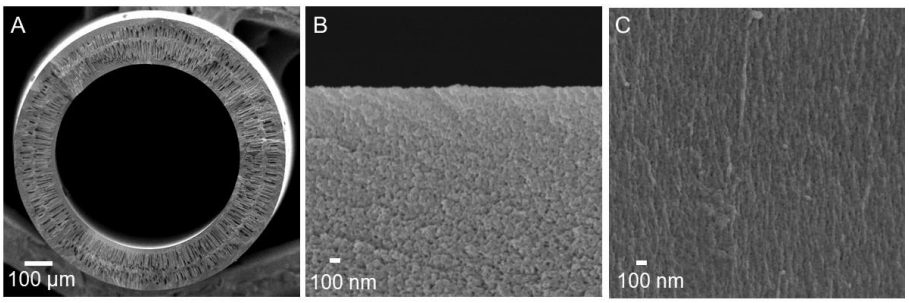

Figure 1: SEM images of hollow fibre substrate. (A) cross-section, (B) enlarged cross-section near lumen (C) inner surface

The chemical compositions of the substrate before and after cross-linking were analysed by comparing their FTIR spectra as shown in Figure 2. The amide peaks, 1634 cm^{-1} and 1525 cm^{-1}, became more intense through the formation of amide groups while imide peaks at 1361 cm^{-1}, 1711 cm^{-1} and 1780 cm^{-1} diminished in intensity after cross-linking. These observations are consistent with previous work and thus, the solvent resistance of the fabricated substrate should perform similarly [17, 37].

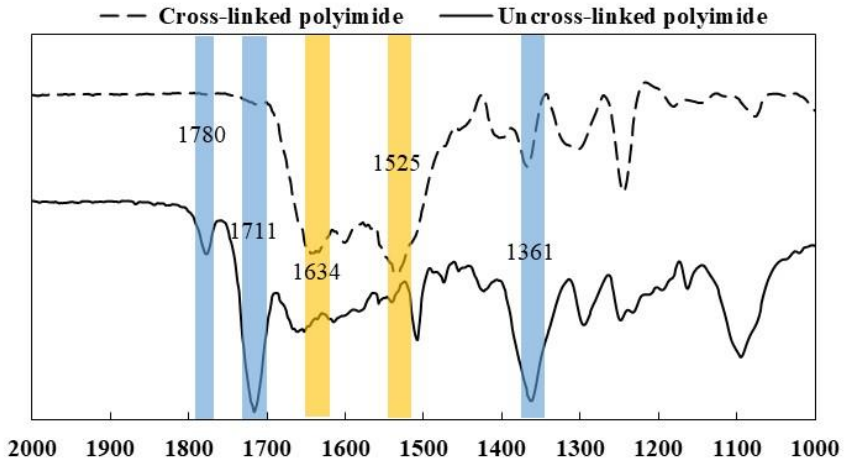

Figure 2: FTIR spectrum of uncross-linked and cross-linked polyimide substrate

The substrate was also tested for organic solvent resistance by immersing it in various organic solvents and measuring the change in mass and length.

Table 3 shows the mass and length changes after immersing the cross-linked membrane in acetone, acetonitrile, IPA and DMF for 7 days. The cross-linked fibres showed negligible loss of mass for all solvents tested. On the other hand, swelling was observed in acetone and DMF at 1% and 6%, respectively. This observation was similar to that previously reported by our group [17]. Thus,

the performance of the hollow fibre substrate was subsequently tested on solvents that did not have much swelling impact.

Table 3: Swelling degree and weight loss for cross-linked membranes in organic solvents for 7 days

Parameter	Solvent	Before immersion (mg)	After immersion (mg)	%
Mass	**Acetone**	74.6 ± 2.4	74.2 ± 2.5	0
	Acetonitrile	74.3 ± 3.3	74.3 ± 3.1	0
	IPA	74.2 ± 1.7	74.3 ± 2.9	0
	DMF	74.4 ± 3.1	74.1 ± 3.6	0.4
Length	**Acetone**	10.0 ± 0.1	10.1 ± 0.2	1
	Acetonitrile	10.0 ± 0.1	10.0 ± 0.1	0
	IPA	10.0 ± 0.1	10.0 ± 0.2	0
	DMF	10.0 ± 0.2	10.6 ± 0.1	6

3.2 Characterisation of polyamide thin-film composite membrane

The SEM images in Figure 3 show the change in morphology on the inner and cross-section of the hollow fibre membrane after IP reaction. From Figure 3(A), the inner surface of the membrane became rougher and was covered by a ridge and valley-like layer, which is characteristic of a polyamide layer. Comparing with our previous work, the MPD-based polyamide layer is thicker than that made from a PEI/PIP-based polyamide layer. Like other polymeric amines, the long-chained PEI yielded a polyamide layer with a lower degree of cross-linking and thus reduced the overall thickness of the selective layer [38]. In the case of pharmaceutical concentration and solvent recovery process, selectivity is much more critical than permeability of the membrane.

Thus, more emphasis was placed on controlling the IP reaction to ensure a defect-free selective layer. As a result, a thicker selective layer was formed to achieve high separation of these expensive pharmaceutical products. The enlarged cross-section of the membrane (Figure 3(b)) shows voluminous voids in the selective layer that is not typically seen in MPD-based membranes for reverse osmosis applications. This might be explained by the lack of high pressure during the testing process, which limits the compaction of the selective layer prior to SEM imaging [39]. Nonetheless, the control of the IP reaction was able to prepare a selective layer onto the 5-piece and 100-piece modules with no noticeable defects.

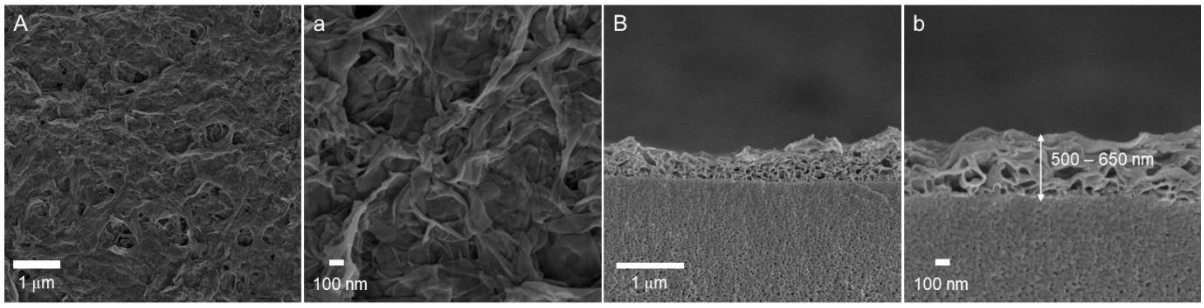

Figure 3: SEM images of TFC membranes, (A) inner surface; (a) enlarged inner surface; (B) cross-section; (b) enlarged cross-section

The changes in surface elemental composition of the substrate and TFC were analysed using XPS as illustrated in Figure 4. From the wide scan XPS spectra in Figure 4(A), it is observed that there is a larger elemental N peak for the TFC membrane compared to the substrate. This can be attributed to the higher concentration of N in polyamide compared to polyimide [17]. The N1s and O1s peaks were deconvoluted into their respective peaks to quantify the chemical bonding present on the surface. From Figure 4(B) and Figure 4(C), the O1s peak for the polyimide substrate can be deconvoluted to O=C-N (531.6 eV) and C=O (532.6 eV), while the peak for the

polyamide thin film can be deconvoluted to O=C-N (531.6 eV) and O=C-O (533.6 eV) [11, 40]. The C=O peak observed in the polyimide substrates was not present after the polyamide layer coating, but a new O=C-O peak was detected. For the N1s peaks, the deconvoluted peaks at 399.1 eV and 400.6 eV correspond to the amide groups and imide rings, respectively [41]. As observed, the amide peak increased after the polyamide layer was applied onto the polyimide substrate. From Table 4, it is observed that the percentage composition of N on the surface increased from 3.96% to 9.02% after the IP reaction. This change was also reported in the previous work where a polyamide selective layer was applied onto P84 substrate [17]. The final elemental composition of the TFC membrane is very similar to those reported in literature of MPD-based polyamide, thus, it indicates that a polyamide layer was successfully applied onto the substrate [18, 19, 30].

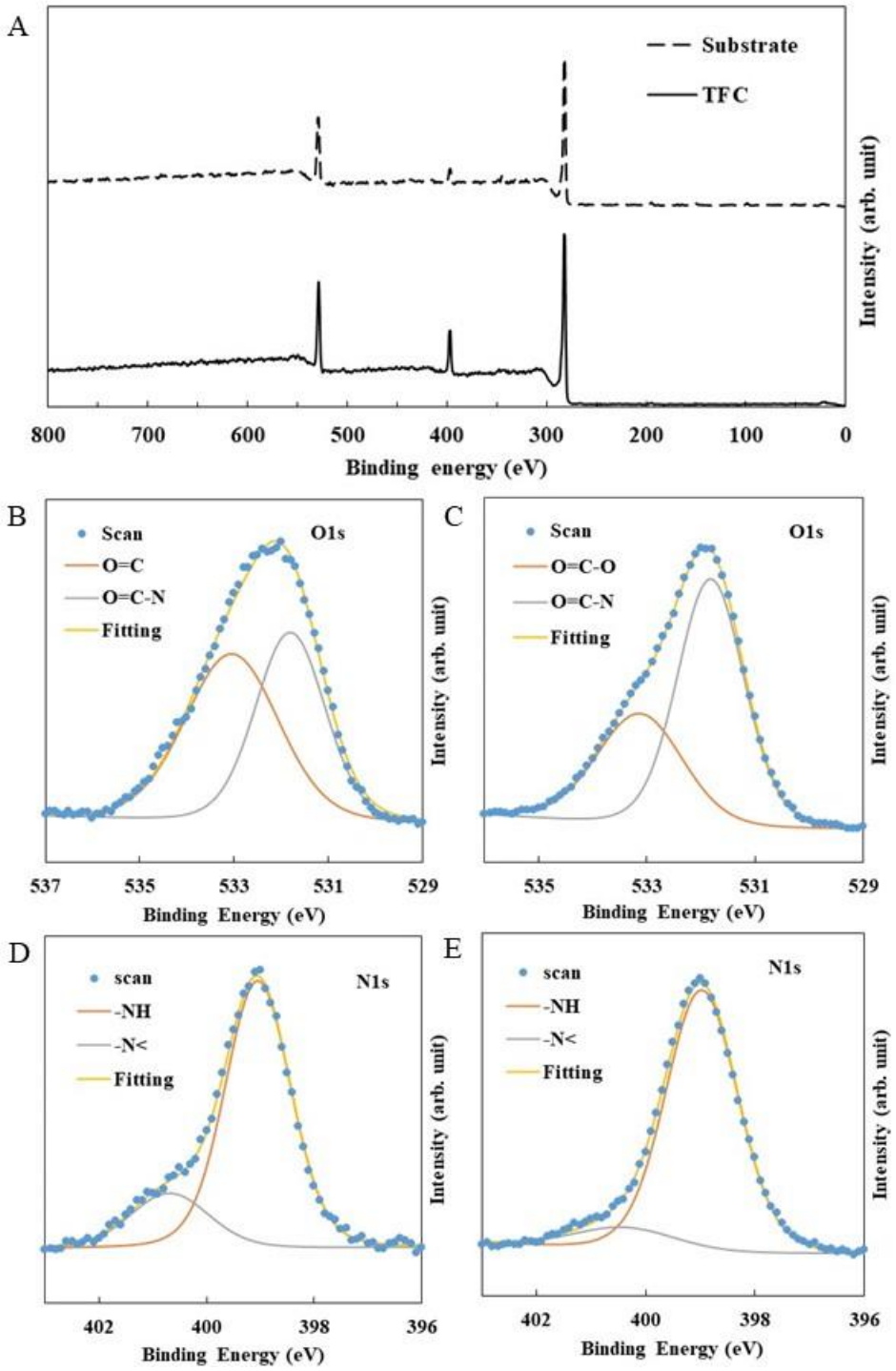

Figure 4: (A) XPS wide scan of polyimide substrate and polyamide TFC membrane, XPS spectra of (B) substrate O1s, (C) TFC O1s, (D) substrate N1s and (E) TFC N1s

Table 4: Elemental composition of substrate and thin-film composite surface by XPS wide scan

Element	Composition (%)	
	Substrate	TFC
O1s	13.66	11.62
C1s	82.38	79.37
N1s	3.96	9.02

3.3 Organic solvent nanofiltration performance

3.3.1 Scalability of hollow fibre membrane

Figure 5 shows the photos of the cross-sections and outside views of the hollow fibre modules. The 100-piece and 5-piece modules have an effective surface area 724 cm^2 and 22 cm^2, respectively. The permeabilities and solute rejections of the modules were compared in Figure 6 and Figure 7, respectively. From Figure 6, it is observed that the pure solvent permeability was reduced when the selective layer was synthesized onto the 100-piece module. To ensure a defect-free selective layer for the large module, the crossflow rate for the IP reaction was tweaked slightly and this may have resulted in lower permeability [30]. However, more emphasis should be placed on the selectivity of the membrane when performing IP reaction section in the context of membrane separation for pharmaceutical processes. In addition, the permeability can be enhanced through solvent activation, which will be discussed in the next section. A more comprehensive study should be done on the effects of scaling up on the performance of hollow fibre membranes to further understand these factors. It is also observed that there is a trend for solvent permeability, where acetone exhibited the highest permeability while ethanol being the

lowest. These observations can usually be explained by the solvents' kinetic diameter (d_{kin}), molar volume, viscosity (η) as well as affinity towards the membrane (δ_{Tot}) (see Table 5) [17, 42-44]. Solvents such as acetone and acetonitrile with lower viscosity and higher affinity to the substrate and selective layer achieve a correspondingly higher permeability as compared to ethanol. On the other hand, the molecular weights and kinetic diameters of the solvents do not seem to explain the permeability trends obtained. From Figure 7, it is observed that the rejections of solutes for the 5-piece and 100-piece modules were relatively similar. Both modules were able to achieve more than 90% rejection to methyl red, indicating a MWCO of less than 269 Da. Compared to the selective layer synthesized using a combination of PEI/PIP monomers in the previous study, the new highly selective layer shows promising potential for pharmaceutical concentration and solvent recovery applications. Upon closer inspection using SEM (Figure 8), it is revealed that a defect-free selective layer was successfully synthesized on the 100-piece module. Thus, the method for synthesizing the polyamide selective layer show promising scalability.

Table 5: Solvent properties [43, 44]

Solvent	**Molecular weight (g mol^{-1})**	**η (mPa s)**	**δ_{Tot} (MPa$^{-1/2}$)**	**d_{kin} (nm)**
Water	18	0.916	47.8	0.265
Ethanol	46	1.081	26.5	0.44
Acetonitrile	41	0.342	24.4	n.a.
Acetone	58	0.34	19.3	0.46

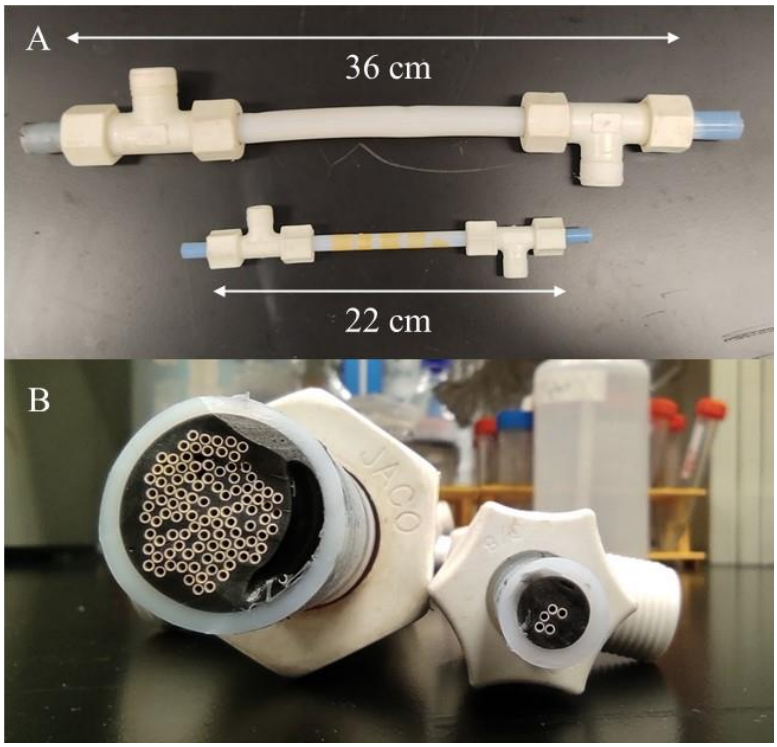

Figure 5: Outside view and cross-section of hollow fibre membrane modules; (A) Outside view of 5-piece and 100-piece modules; (B) Cross-section of 5-piece and 100-piece modules

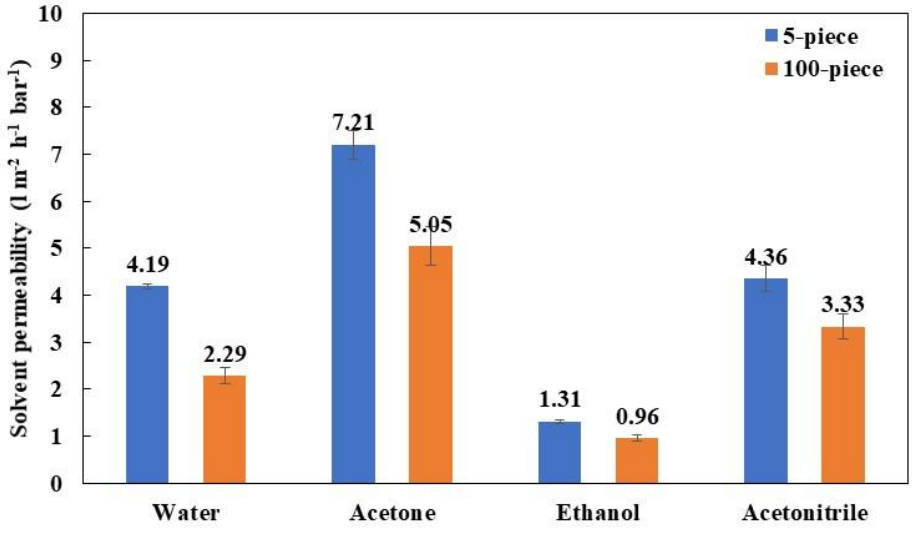

Figure 6: Solvent permeability comparisons for 5-piece and 100-piece modules

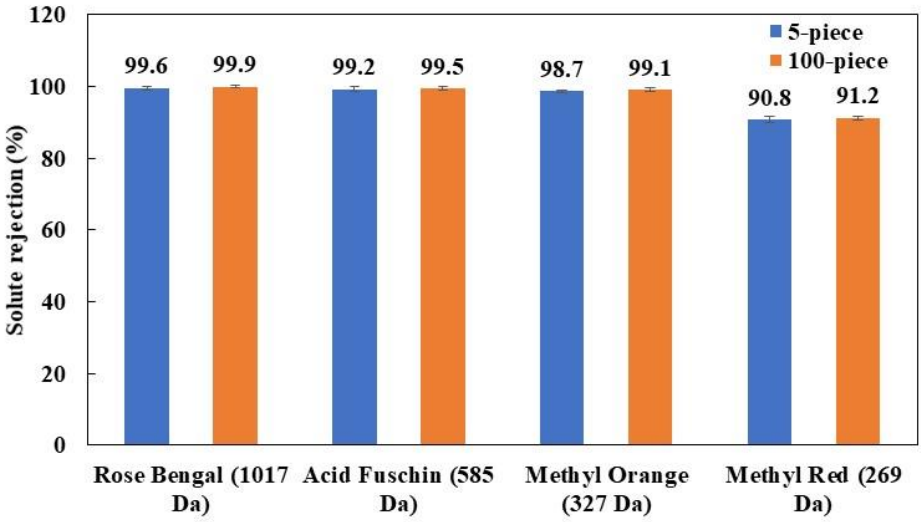

Figure 7: Solutes rejections comparisons for 5-piece and 100-piece modules in acetone

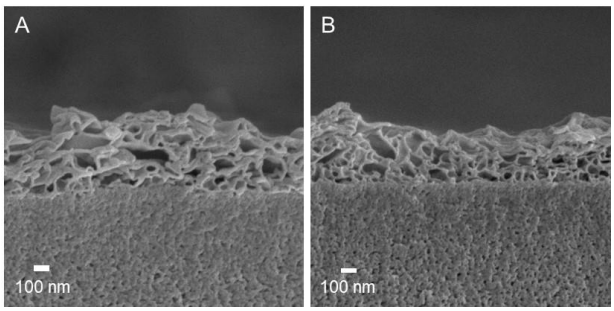

Figure 8: SEM images of the inner surface of the 100-piece module; (A) inlet of the module, (B) outlet of the module

3.3.2 Extended filtration test for pristine 100-piece module

A 7-day OSN filtration experiment was done on the pristine 100-piece module to evaluate its stability in OSN application. As observed from Figure 9, the acetone permeability remained stable at about 5.1 l m^{-2} h^{-1} bar^{-1} while methyl red rejection kept constant at about 91.2%. This suggests that the performance of the membrane can be maintained for an extended period. However, given

the low concentration of solute used in the test, the potential fouling issue should be further studied to understand the impact of fouling on its performance.

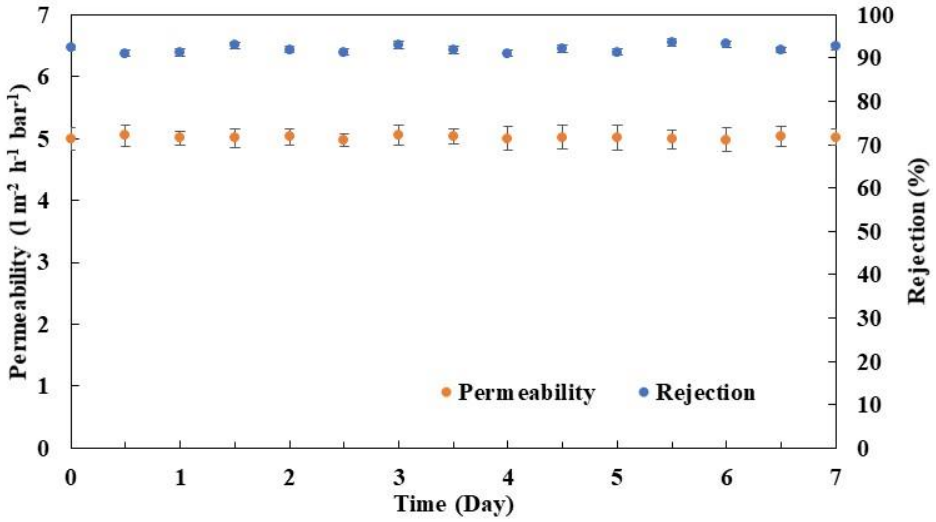

Figure 9: 7-day filtration test for 100-piece module (50 ppm of methyl red in acetone at 2 bar)

3.3.3 Solvent activation of 100-piece module

To increase the permeability of the 100-piece module, it was subsequently activated by DMF. Figure 10 shows the SEM images of the pristine and solvent-activated membrane. The surface morphology of the selective layer did not show much noticeable change after activation as shown by Figure 10(A) and Figure 10(a). However, there is a noticeable increase in voids in the polyamide layer as shown in the cross-sections after solvent activation (Figure 10(B) and Figure 10(b)). As DMF is one of the top swelling solvents for aromatic polyamides, the polyamide layer might has been swollen and those smaller and uncross-linked molecular fragments were washed away by the entry of DMF into the membrane matrix [14, 45]. It can also be observed that there is a visible increase in porosity of the substrate, which can be explained by the slight loss of mass during the weight-loss experiment. Some uncross-linked polyimide polymers in the substrate may have also been dissolved by DMF, unblocking the membrane pores and potentially increasing the overall permeability of the TFC membrane [14, 45].

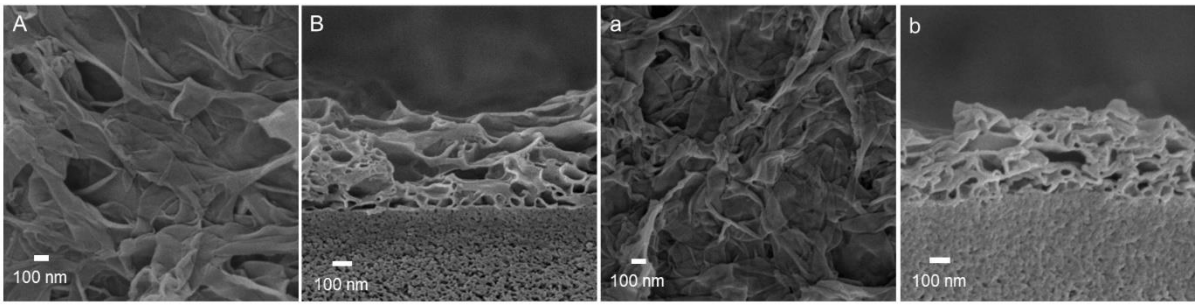

Figure 10: SEM images of pristine and solvent-activated membrane. (A) Inner surface; and (B) cross-section of solvent-activated membrane; (a) Inner surface; and (b) cross-section of pristine membrane.

The permeability and solute rejection of the pristine and solvent-activated membranes were compared and the results are shown in Figure 11 and Figure 12. As predicted, there is a significant increase in solvent permeability after solvent activation. Notably, acetone permeability increased dramatically by about 4.8 times from 5.1 l m^{-2} h^{-1} bar^{-1} to 24.3 l m^{-1} h^{-1} bar^{-1}. On the other hand, the collapsing of the pores on the surface due to lower polymer matrix modulus were able to maintain the rejections of the solutes [14]. This shows potential for scale-up modules to use solvent activation as an effective approach to enhance permeability without the trade-off of much lower selectivity. However, a thorough analysis of solvent-activated membranes should be performed to ensure stable OSN performance over a long period of operation.

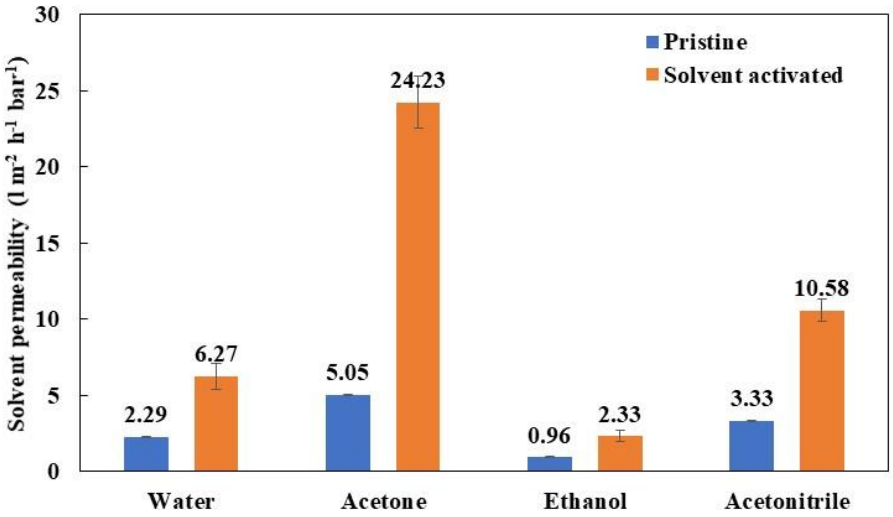

Figure 11: Solvent permeability of pristine and solvent-activated membranes

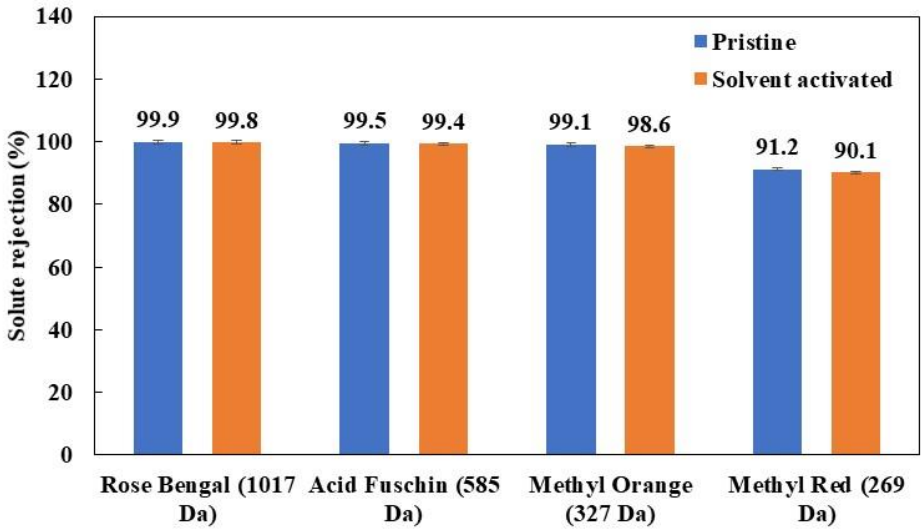

Figure 12: Solute rejection of pristine and solvent-activated membranes

A 7-day organic solvent filtration experiment was performed for the solvent-activated membrane and the performance is shown in Figure 13. As observed, the membrane was able to maintain about 90% of methyl red rejection throughout the 7-day period. However, this is slightly lower than that attained by the non-activated membrane (~91.2%). This might be caused by the slight dissolution of the selective layer during the solvent activation process, negatively affecting its selectivity. On the other hand, the membrane can maintain a high permeability about 23.5 l m^{-2} h^{-}

^{1} bar^{-1} throughout the experiment. This demonstrates that solvent activation is an effective way to improve membrane performance, but the degree of the solvent activation needs to be controlled carefully. After all, the selectivity of a membrane plays a more important role in pharmaceutical industries due to the high value of KOMs [46], especially when industries seek for high quality in its products.

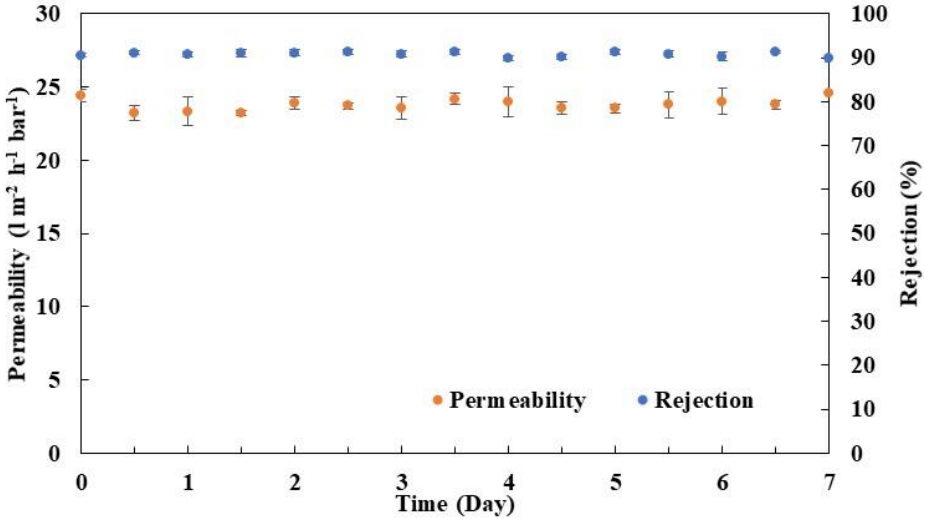

Figure 13: 7-day filtration test for solvent-activated 100-piece module (50 ppm of methyl red in acetone at 2 bar)

3.3.4 Concentration of levofloxacin and solvent recovery

The capability of the 100-piece modules for concentrating API was demonstrated by performing a single-pass batch process using levofloxacin as a model API. The permeate was collected and stored in a separate tank while the retentate was recirculated back into the feed tank. Consequently, the volume of feed reduces, thereby increasing the concentration of API in the feed. Levofloxacin (361 Da), an antibiotic, was dissolved in acetone as feed for the experiment. Acetone was used as the solvent for this experiment as it is one of the commonly used solvents in manufacturing and pharmaceutical industries [1, 47]. In addition, levofloxacin is highly soluble in acetone. The permeability of acetone and rejection of levofloxacin were measured periodically, and the data

obtained for the pristine and solvent-activated 100-piece module were plotted against time as shown in Figure 14. As observed, the initial rejection for the pristine membrane was maintained at about 99.2% for more than 9 hours of operations. Subsequently, there was a decrease in rejection to about 95% when the feed concentration was increased from 5,000 ppm to 20,000 ppm. This might be caused by concentration polarisation at the membrane boundary due to higher API concentrations. The rejection of the pristine membrane gradually decreases towards the end of the experiment when the concentration reaches 20,000 ppm. Similarly, the solvent-activated membrane also suffered a drop in rejection as the concentration of feed increased. An initial rejection of about 98.2% for the solvent-activated membrane gradually decreased to 94.1% at the end of the experiment, indicating that concentration polarisation is affecting its performance.

On the other hand, the solvent permeability of the pristine membrane also dropped drastically from 5.1 l m^{-2} h^{-1} bar^{-1} to 1.5 l m^{-2} h^{-1} bar^{-1} over the course of the experiment. This further implies that fouling might have occurred on the membrane surfaces, reducing its permeability. Similar observation was also made on the solvent-activated membranes. An initial permeability of 16.2 l m^{-2} h^{-1} bar^{-1} was gradually reduced to 6.21 l m^{-2} h^{-1} bar^{-1} within 6 hours of operation. Obviously, the higher permeability of the solvent-activated membrane resulted in a faster rate of concentration of the same amount of feed. This reduces the time taken for a batch process to complete. As demonstrated, the membrane was able to concentrate the API to 20,000 ppm from a low concentration. An even higher concentration of API can then be obtained by using conventional methods of purification. In addition, more than 95% of acetone was recovered in each of the experiment. To reuse the recovered solvent, further polishing steps are required to remove the trace amount of levofloxacin, but it is beyond the scope of current study.

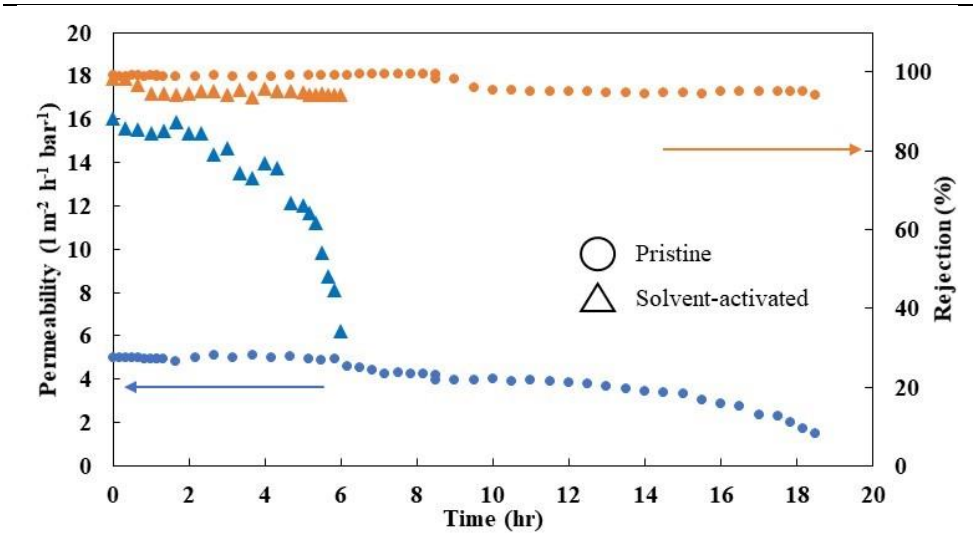

Figure 14: Levofloxacin concentration and solvent recovery - rejection and permeability for pristine and solvent-activated 100-piece module

To determine if the fouling was reversible, the modules were flushed with pure acetone at 2 bar for 1 hour at the end of the concentration experiment before measuring their performances again. It turned out that the modules were able to maintain 91% methyl red rejection and recovered more than 95% of their initial acetone permeability. This suggests that the fouling of the 100-piece modules by levofloxacin during the concentration experiment did not have much permanent impact on their performances. , It demonstrates that the OSN membrane can potentially be used to recover solvents from process streams in the pharmaceutical industries. Its high selectivity would also allow it to be used as a polishing step to remove trace amount of contaminants in the recovered solvent through multi-step filtration process. In addition, it can also be employed as a pre-treatment for distillation during API purification processes. The filtration removes the main bulk of the intermediate stream, leaving a more concentrated pharmaceutical intermediate stream with a much lower volume, thereby reducing the energy required to heat the organic solvent during the distillation process. However, fouling is still a prevalent issue that needs to be addressed, similar to any membrane–based process, but this issue is not the focus of current study.

3.3.5 Performance comparison of solvent-activated membrane and commercial membranes

The performance of the solvent-activated 100-piece module was compared with several OSN membranes in Table 6. Most of the membranes shown in the table are in flatsheet configuration. On the other hand, the membrane fabricated in this work is of hollow fibre configuration, which offers higher packing density and self-supporting capability. For the solvent-activated membrane, the ethanol permeability was able to match most OSN membranes reported in literature at 2.33 l m^{-2} h^{-1} bar^{-1}. The acetone permeability also increased significantly compared with our previous study (24.2 vs 11.6 l m^{-2} h^{-1} bar^{-1}). In addition, the selectivity of the solvent-activated membrane performed much better than most of the other membranes mentioned in the table, with a MWCO of about 269 Da. For example, the solvent-activated membrane achieved comparable rejection to NH_2-MWCNT/PI membrane while having a significantly higher acetone permeability.

The prolonged testing of the 100-piece module in this study also suggests that the solvent activation step is a promising approach. In addition, the polyamide selective layer was successfully synthesized for not only the 5-piece module but also for the 100-piece hollow fibre module with membrane surface area of 724 cm^2, demonstrating the feasibility of scaling up the technology. Overall, the facile and scalable membrane fabricated in this work was able to match, if not outperform, many of the state-of-the-art OSN membranes.

Table 6: OSN membrane performance of recent works and 100-piece module developed in this work

Membrane	Membrane size (cm^2)	Configuration	Solvent	Permeability ($l\ m^{-2}\ h^{-1}\ bar^{-1}$)	Solute	Molecular weight (Da)	Rejection (%)	[Ref] Year
(Catechol/POSS)/PI	21.2	Flatsheet	Ethanol	1.26	Rose Bengal	1017	99	[48] 2017
PAN	19	Hollow fibre	Ethanol	2.32	Remazol brilliant blue R	626	99.9	[49] 2017
Pebax/PAN	12.6	Flatsheet	Ethanol	1.9	Brilliant blue R	826	95	[50] 2017
Cellulose	6	Flatsheet	Ethanol	0.3	Brilliant blue R	826	94.0	[51] 2018
Kevlar	14.6	Flatsheet	Ethanol	2.9	Rose Bengal	1017	95	[52] 2019
sPPSU-ECH	9.62	Flatsheet	Ethanol	11.9	Brilliant blue R Eosin Y Tetracycline	826 645 444	96 95 76.8	[53] 2019
mZIF-8 TFC/PI	28.26	Flatsheet	Ethanol	2.8	Rhodamine B	479	99.1	[54] 2020
GQDs-PEI	-	Flatsheet	Ethanol	4.03	Rhodamine B	479	98.7	[55] 2020
$(FPA\text{-}0.5/PI)_{xa}$	28.26	Flatsheet	Ethanol	4.16	Rhodamine B	479	99.4	[56] 2019
NH_2-MWCNT/PI	-	Hollow fibre	Acetone	4.31	Brilliant blue R	826	99.9	[57] 2018
PEI/PIP-based TFC/PI	32	Hollow fibre	Acetone	11.6	Acid fuchsin Methyl orange	585 327	91.8 46.5	[17] 2020
MPD-based TFC/PI (Solvent-activated)	724	Hollow fibre	Acetone Ethanol Acetonitrile	24.2 ± 1.7 2.33 ± 0.36 10.58 ± 0.75	Acid fuchsin Methyl orange Methyl red	585 327 269	99.4 98.6 90.1	This work

	Levofloxacin	361	98.2

4. Conclusions

In this study, a hollow fibre thin-film composite membrane was developed and scaled up by increasing the packing density through changes in spinning parameters. An RO-like selective layer was synthesized to achieve higher selectivity for pharmaceutical applications. Subsequently, solvent activation was applied to enhance permeability while maintaining high solute selectivity. Consequently, the solvent-activated membrane was able to achieve significantly higher permeability of various organic solvents than the pristine membrane, without compromising on its selectivity. In addition, it also demonstrated excellent stability in acetone under operating conditions over a period of 7 days. This demonstrates the scalability of the thin-film composite fabrication and uses of solvent activation for improved performance. The fabricated membrane also exhibited promising performance in the batch-processed concentration experiment of levofloxacin in acetone, reaffirming its potential for use in pharmaceutical OSN application.

Acknowledgements

The authors acknowledge Economic Development Board (EDB) of Singapore for funding the Singapore Membrane Technology Centre (SMTC), Interdisciplinary Graduate Programme, Nanyang Environment and Water Research Institute, Nanyang Technological University.

Notes

The authors declare no competing financial interest.

Authors Statement:

Keng Siang Goh: Investigation, Data Curation, Writing - Original Draft

Yunfeng Chen & Jeng Yi: Resources, Writing - Review & Editing

T.-H Bae: Supervision

Rong Wang: Writing - Supervision, Review & Editing, Project Administration, Funding Acquisition

References

[1] K. Grodowska, A. Parczewski, Organic solvents in the pharmaceutical industry, Acta poloniae pharmaceutica, 67 (2010) 3-12.
[2] Y. Cui, T.-S. Chung, Pharmaceutical concentration using organic solvent forward osmosis for solvent recovery, Nature Communications, 9 (2018) 1426.
[3] P. Marchetti, M.F. Jimenez Solomon, G. Szekely, A.G. Livingston, Molecular separation with organic solvent nanofiltration: A critical review, Chemical Reviews, 114 (2014) 10735-10806.
[4] R.P. Lively, D.S. Sholl, From water to organics in membrane separations, Nature Materials, 16 (2017) 276-279.
[5] Y.H. See Toh, F.W. Lim, A.G. Livingston, Polymeric membranes for nanofiltration in polar aprotic solvents, Journal of Membrane Science, 301 (2007) 3-10.
[6] D.S. Sholl, R.P. Lively, Seven chemical separations to change the world, Nature, 532 (2016) 435-437.
[7] P. Vandezande, L.E.M. Gevers, I.F.J. Vankelecom, Solvent resistant nanofiltration: separating on a molecular level, Chemical Society Reviews, 37 (2008) 365-405.
[8] K. Vanherck, G. Koeckelberghs, I.F.J. Vankelecom, Crosslinking polyimides for membrane applications: A review, Progress in Polymer Science, 38 (2013) 874-896.
[9] S.K. Lim, K. Goh, T.-H. Bae, R. Wang, Polymer-based membranes for solvent-resistant nanofiltration: A review, Chinese Journal of Chemical Engineering, 25 (2017) 1653-1675.
[10] D. Fritsch, P. Merten, K. Heinrich, M. Lazar, M. Priske, High performance organic solvent nanofiltration membranes: Development and thorough testing of thin film composite membranes made of polymers of intrinsic microporosity (PIMs), Journal of Membrane Science, 401-402 (2012) 222-231.
[11] C. Li, S. Li, L. Lv, B. Su, M.Z. Hu, High solvent-resistant and integrally crosslinked polyimide-based composite membranes for organic solvent nanofiltration, Journal of Membrane Science, 564 (2018) 10-21.
[12] Evonik, DURAMEM® AND PURAMEM® MEMBRANES FOR ORGANIC SOLVENT NANOFILTRATION, in.
[13] H. Mariën, I.F.J. Vankelecom, Transformation of cross-linked polyimide UF membranes into highly permeable SRNF membranes via solvent annealing, Journal of Membrane Science, 541 (2017) 205-213.
[14] M.F. Jimenez Solomon, Y. Bhole, A.G. Livingston, High flux membranes for organic solvent nanofiltration (OSN)—Interfacial polymerization with solvent activation, Journal of Membrane Science, 423-424 (2012) 371-382.
[15] M. Amirilargani, M. Sadrzadeh, E.J.R. Sudhölter, L.C.P.M. de Smet, Surface modification methods of organic solvent nanofiltration membranes, Chemical Engineering Journal, 289 (2016) 562-582.
[16] A.W. Mohammad, Y.H. Teow, W.L. Ang, Y.T. Chung, D.L. Oatley-Radcliffe, N. Hilal, Nanofiltration membranes review: Recent advances and future prospects, Desalination, 356 (2015) 226-254.
[17] K.S. Goh, J.Y. Chong, Y. Chen, W. Fang, T.-H. Bae, R. Wang, Thin-film composite hollow fibre membrane for low pressure organic solvent nanofiltration, Journal of Membrane Science, 597 (2020) 117760.
[18] B. Khorshidi, T. Thundat, B.A. Fleck, M. Sadrzadeh, Thin film composite polyamide membranes: parametric study on the influence of synthesis conditions, RSC Advances, 5 (2015) 54985-54997.

[19] B. Khorshidi, T. Thundat, B.A. Fleck, M. Sadrzadeh, A Novel Approach Toward Fabrication of High Performance Thin Film Composite Polyamide Membranes, Scientific Reports, 6 (2016) 22069.
[20] J.H. Kim, S.J. Moon, S.H. Park, M. Cook, A.G. Livingston, Y.M. Lee, A robust thin film composite membrane incorporating thermally rearranged polymer support for organic solvent nanofiltration and pressure retarded osmosis, Journal of Membrane Science, 550 (2018) 322-331.
[21] A. LIVINGSTON, L. PEEVA, S. HAN, D. NAIR, S.S. LUTHRA, L.S. WHITE, L.M. FREITAS DOS SANTOS, Membrane Separation in Green Chemical Processing, Annals of the New York Academy of Sciences, 984 (2003) 123-141.
[22] J.P. Sheth, Y. Qin, K.K. Sirkar, B.C. Baltzis, Nanofiltration-based diafiltration process for solvent exchange in pharmaceutical manufacturing, Journal of Membrane Science, 211 (2003) 251-261.
[23] L.S. White, Development of large-scale applications in organic solvent nanofiltration and pervaporation for chemical and refining processes, Journal of Membrane Science, 286 (2006) 26-35.
[24] L.S. White, A.R. Nitsch, Solvent recovery from lube oil filtrates with a polyimide membrane, Journal of Membrane Science, 179 (2000) 267-274.
[25] J. Vanneste, D. Ormerod, G. Theys, D. Van Gool, B. Van Camp, S. Darvishmanesh, B. Van der Bruggen, Towards high resolution membrane-based pharmaceutical separations, Journal of Chemical Technology & Biotechnology, 88 (2013) 98-108.
[26] R.M. Gould, L.S. White, C.R. Wildemuth, Membrane separation in solvent lube dewaxing, Environmental Progress, 20 (2001) 12-16.
[27] D. Ott, D. Kralisch, I. Denčić, V. Hessel, Y. Laribi, P.D. Perrichon, C. Berguerand, L. Kiwi-Minsker, P. Loeb, Life Cycle Analysis within Pharmaceutical Process Optimization and Intensification: Case Study of Active Pharmaceutical Ingredient Production, ChemSusChem, 7 (2014) 3521-3533.
[28] D.L. Zhao, S. Japip, Y. Zhang, M. Weber, C. Maletzko, T.-S. Chung, Emerging thin-film nanocomposite (TFN) membranes for reverse osmosis: A review, Water Research, 173 (2020) 115557.
[29] R. Mukherjee, P. Bhunia, S. De, Long term filtration modelling and scaling up of mixed matrix ultrafiltration hollow fiber membrane: a case study of chromium(VI) removal, Journal of Membrane Science, 570-571 (2019) 204-214.
[30] Y. Chen, C.H. Loh, L. Zhang, L. Setiawan, Q. She, W. Fang, X. Hu, R. Wang, Module scale-up and performance evaluation of thin film composite hollow fiber membranes for pressure retarded osmosis, Journal of Membrane Science, 548 (2018) 398-407.
[31] D. Li, R. Wang, T.-S. Chung, Fabrication of lab-scale hollow fiber membrane modules with high packing density, Separation and Purification Technology, 40 (2004) 15-30.
[32] S.K. Lim, L. Setiawan, T.-H. Bae, R. Wang, Polyamide-imide hollow fiber membranes crosslinked with amine-appended inorganic networks for application in solvent-resistant nanofiltration under low operating pressure, Journal of Membrane Science, 501 (2016) 152-160.
[33] L. Shi, S.R. Chou, R. Wang, W.X. Fang, C.Y. Tang, A.G. Fane, Effect of substrate structure on the performance of thin-film composite forward osmosis hollow fiber membranes, Journal of Membrane Science, 382 (2011) 116-123.
[34] M. Rahbari-sisakht, A.F. Ismail, T. Matsuura, Effect of bore fluid composition on structure and performance of asymmetric polysulfone hollow fiber membrane contactor for CO2 absorption, Separation and Purification Technology, 88 (2012) 99-106.

[35] N.Y. Yip, A. Tiraferri, W.A. Phillip, J.D. Schiffman, M. Elimelech, High Performance Thin-Film Composite Forward Osmosis Membrane, Environmental Science & Technology, 44 (2010) 3812-3818.
[36] A. Tiraferri, N.Y. Yip, W.A. Phillip, J.D. Schiffman, M. Elimelech, Relating performance of thin-film composite forward osmosis membranes to support layer formation and structure, Journal of Membrane Science, 367 (2011) 340-352.
[37] K. Vanherck, P. Vandezande, S.O. Aldea, I.F.J. Vankelecom, Cross-linked polyimide membranes for solvent resistant nanofiltration in aprotic solvents, Journal of Membrane Science, 320 (2008) 468-476.
[38] W. Fang, L. Shi, R. Wang, Mixed polyamide-based composite nanofiltration hollow fiber membranes with improved low-pressure water softening capability, Journal of Membrane Science, 468 (2014) 52-61.
[39] Y. Chen, L. Setiawan, S. Chou, X. Hu, R. Wang, Identification of safe and stable operation conditions for pressure retarded osmosis with high performance hollow fiber membrane, Journal of Membrane Science, 503 (2016) 90-100.
[40] S.-H. Park, Y.-S. Ko, S.-J. Park, J.S. Lee, J. Cho, K.-Y. Baek, I.T. Kim, K. Woo, J.-H. Lee, Immobilization of silver nanoparticle-decorated silica particles on polyamide thin film composite membranes for antibacterial properties, Journal of Membrane Science, 499 (2016) 80-91.
[41] D.W. Mangindaan, N.M. Woon, G.M. Shi, T.S. Chung, P84 polyimide membranes modified by a tripodal amine for enhanced pervaporation dehydration of acetone, Chemical Engineering Science, 122 (2015) 14-23.
[42] D.o.R. Machado, D. Hasson, R. Semiat, Effect of solvent properties on permeate flow through nanofiltration membranes. Part I: investigation of parameters affecting solvent flux, Journal of Membrane Science, 163 (1999) 93-102.
[43] A. Buekenhoudt, F. Bisignano, G. De Luca, P. Vandezande, M. Wouters, K. Verhulst, Unravelling the solvent flux behaviour of ceramic nanofiltration and ultrafiltration membranes, Journal of Membrane Science, 439 (2013) 36-47.
[44] S. Darvishmanesh, J. Degrève, B. Van der Bruggen, Mechanisms of solute rejection in solvent resistant nanofiltration: the effect of solvent on solute rejection, Physical Chemistry Chemical Physics, 12 (2010) 13333-13342.
[45] M.F. Jimenez Solomon, Y. Bhole, A.G. Livingston, High flux hydrophobic membranes for organic solvent nanofiltration (OSN)—Interfacial polymerization, surface modification and solvent activation, Journal of Membrane Science, 434 (2013) 193-203.
[46] P. Marchetti, L. Peeva, A. Livingston, The Selectivity Challenge in Organic Solvent Nanofiltration: Membrane and Process Solutions, Annual Review of Chemical and Biomolecular Engineering, 8 (2017) 473-497.
[47] S. Wang, D. Mahalingam, B. Sutisna, S.P. Nunes, 2D-dual-spacing channel membranes for high performance organic solvent nanofiltration, Journal of Materials Chemistry A, 7 (2019) 11673-11682.
[48] Y.C. Xu, Y.P. Tang, L.F. Liu, Z.H. Guo, L. Shao, Nanocomposite organic solvent nanofiltration membranes by a highly-efficient mussel-inspired co-deposition strategy, Journal of Membrane Science, 526 (2017) 32-42.
[49] Hui M. Tham, K.Y. Wang, D. Hua, S. Japip, T.-S. Chung, From ultrafiltration to nanofiltration: Hydrazine cross-linked polyacrylonitrile hollow fiber membranes for organic solvent nanofiltration, Journal of Membrane Science, 542 (2017) 289-299.
[50] J. Aburabie, K.-V. Peinemann, Crosslinked poly(ether block amide) composite membranes for organic solvent nanofiltration applications, Journal of Membrane Science, 523 (2017) 264-272.

[51] F.M. Sukma, P.Z. Çulfaz-Emecen, Cellulose membranes for organic solvent nanofiltration, Journal of Membrane Science, 545 (2018) 329-336.
[52] S. Yuan, J. Swartenbroekx, Y. Li, J. Zhu, F. Ceyssens, R. Zhang, A. Volodine, J. Li, P. Van Puyvelde, B. Van der Bruggen, Facile synthesis of Kevlar nanofibrous membranes via regeneration of hydrogen bonds for organic solvent nanofiltration, Journal of Membrane Science, 573 (2019) 612-620.
[53] Y. Feng, M. Weber, C. Maletzko, T.-S. Chung, Fabrication of organic solvent nanofiltration membranes via facile bioinspired one-step modification, Chemical Engineering Science, 198 (2019) 74-84.
[54] S. Yang, H. Li, X. Zhang, S. Du, J. Zhang, B. Su, X. Gao, B. Mandal, Amine-functionalized ZIF-8 nanoparticles as interlayer for the improvement of the separation performance of organic solvent nanofiltration (OSN) membrane, Journal of Membrane Science, 614 (2020) 118433.
[55] Y. Liang, C. Li, S. Li, B. Su, M.Z. Hu, X. Gao, C. Gao, Graphene quantum dots (GQDs)-polyethyleneimine as interlayer for the fabrication of high performance organic solvent nanofiltration (OSN) membranes, Chemical Engineering Journal, 380 (2020) 122462.
[56] Y. Guo, S. Li, B. Su, B. Mandal, Fluorine incorporation for enhancing solvent resistance of organic solvent nanofiltration membrane, Chemical Engineering Journal, 369 (2019) 498-510.
[57] M.H. Davood Abadi Farahani, T.-S. Chung, Solvent resistant hollow fiber membranes comprising P84 polyimide and amine-functionalized carbon nanotubes with potential applications in pharmaceutical, food, and petrochemical industries, Chemical Engineering Journal, 345 (2018) 174-185.